AFRL-RZ-ED-TR-2007-0065 AFRL-RZ-ED-TR-2007-0065

Kinetic Modeling of Laser-Induced Fusion

Peter Messmer
Kevin Paul
Peter Stoltz
Tech-X Corporation
5621 Arapahoe Ave., Suite A
Boulder CO 80303

Jean-Luc Cambier
AFRL/RZSA
10 E. Saturn Blvd.
Edwards AFB CA 93524-7680

September 2007

Special Report

APPROVED FOR PUBLIC RELEASE; DISTRIBUTION UNLIMITED.

AIR FORCE RESEARCH LABORATORY
AIR FORCE MATERIEL COMMAND
EDWARDS AIR FORCE BASE CA 93524-7048

UNCLASSIFIED

REPORT DOCUMENTATION PAGE

Form Approved
OMB No. 0704-0188

Public reporting burden for this collection of information is estimated to average 1 hour per response, including the time for reviewing instructions, searching existing data sources, gathering and maintaining the data needed, and completing and reviewing this collection of information. Send comments regarding this burden estimate or any other aspect of this collection of information, including suggestions for reducing this burden to Department of Defense, Washington Headquarters Services, Directorate for Information Operations and Reports (0704-0188), 1215 Jefferson Davis Highway, Suite 1204, Arlington, VA 22202-4302. Respondents should be aware that notwithstanding any other provision of law, no person shall be subject to any penalty for failing to comply with a collection of information if it does not display a currently valid OMB control number. **PLEASE DO NOT RETURN YOUR FORM TO THE ABOVE ADDRESS.**

1. REPORT DATE *(DD-MM-YYYY)* 01-07-2007	**2. REPORT TYPE** Special Report	**3. DATES COVERED** *(From - To)* 31 Jul 2002 – 24 Sep 2007
4. TITLE AND SUBTITLE Kinetic Modeling of Laser Induced Fusion		**5a. CONTRACT NUMBER** RP060281
		5b. GRANT NUMBER
		5c. PROGRAM ELEMENT NUMBER 61102F
6. AUTHOR(S) Peter Messmer, Kevin Paul, Peter Stoltz, Jean-Luc Cambier*		**5d. PROJECT NUMBER**
		5e. TASK NUMBER
		5f. WORK UNIT NUMBER 23040256
7. PERFORMING ORGANIZATION NAME(S) AND ADDRESS(ES) Tech-X Corporation 5621 Arapahoe Ave., Suite A Boulder CO 80303		**8. PERFORMING ORGANIZATION REPORT NO.**
9. SPONSORING / MONITORING AGENCY NAME(S) AND ADDRESS(ES) Air Force Research Laboratory (AFMC) *AFRL/RZSA 10 E. Saturn Blvd. Edwards AFB CA 93524-7680		**10. SPONSOR/MONITOR'S ACRONYM(S)**
		11. SPONSOR/MONITOR'S REPORT NUMBER(S) **AFRL-RZ-ED-TR-2007-0065**

12. DISTRIBUTION / AVAILABILITY STATEMENT
Approved for public release; distribution unlimited. Public Affairs No. 07298A.

13. SUPPLEMENTARY NOTES

14. ABSTRACT

Thermal neutrons are of considerable interest to the Department of Defense and for commercial applications. Unlike high-energy photons, neutrons easily penetrate high density targets, but get effectively absorbed by low density materials like paraffin, nylon or explosives. This makes them attractive complements to X-rays for radiographic applications, e.g. for the detection or inspection of explosives inside steel casings. The key challenge is to develop a compact generator for thermal neutrons with large enough flux. The limited availability of radio-isotopes, combined with the relatively short half-life, safety constraints and regulatory requirements make them unattractive for wide-spread use. An alternative design exploits the Deuterium-Tritium (D-T) fusion, which generates Alpha particles and fast neutrons. In these sources, Deuterium ions are accelerated to about 130 keV and hit a Tritium target. The acceleration of Deuterium ions is usually accomplished in a diode configuration. Recently, considerable success has been achieved in the acceleration of ions via laser-matter interaction. In this project we investigated whether laser-accelerated ions could undergo nuclear fusion in an adequately designed target and could be used for neutron sources. We therefore enhanced our proprietary plasma simulation code VORPAL with a model for fusion reactions and investigated the generation of neutrons in shaped D-T targets. We find that neutron fluxes large enough for radiographic applications can be generated by utilizing moderate ($\approx 10^{17}$–10^{18} W/cm^2) laser intensities.

15. SUBJECT TERMS
Laser; fusion; kinetic; modeling; thermal neutrons; deuterium; VORPAL

16. SECURITY CLASSIFICATION OF:			**17. LIMITATION OF ABSTRACT**	**18. NUMBER OF PAGES**	**19a. NAME OF RESPONSIBLE PERSON**
					Dr. Jean-Luc J. Cambier
a. REPORT	**b. ABSTRACT**	**c. THIS PAGE**	SAR	27	**19b. TELEPHONE NO** *(include area code)*
Unclassified	**Unclassified**	**Unclassified**			N/A

Standard Form 298 (Rev. 8-98)
Prescribed by ANSI Std. 239.18

STINFO COPY
NOTICE AND SIGNATURE PAGE

Using Government drawings, specifications, or other data included in this document for any purpose other than Government procurement does not in any way obligate the U.S. Government. The fact that the Government formulated or supplied the drawings, specifications, or other data does not license the holder or any other person or corporation; or convey any rights or permission to manufacture, use, or sell any patented invention that may relate to them.

Qualified requestors may obtain copies of this report from the Defense Technical Information Center (DTIC) (http://www.dtic.mil).

AFRL-RZ-ED-TR-2007-0065 HAS BEEN REVIEWED AND IS APPROVED FOR PUBLICATION IN ACCORDANCE WITH ASSIGNED DISTRIBUTION STATEMENT.

FOR THE DIRECTOR:

____//signed//_____
JEAN-LUC J. CAMBIER
Project Manager

____//signed//_____
INGRID J. WYSONG
Chief, Aerophysics Branch

____//signed//_____
PHILIP A. KESSEL
Technical Advisor
Space & Missile Propulsion Division

This report is published in the interest of scientific and technical information exchange, and its publication does not constitute the Government's approval or disapproval of its ideas or findings.

Kinetic Modeling of Laser Induced Fusion

Final Report

Contract # RP060281

Peter Messmer, Kevin Paul, Peter Stoltz
Tech-X Corporation

Jean-Luc Cambier
AFRL

PREPARED BY:

Tech-X Corporation
5621 Arapahoe Avenue, Suite A
Boulder, CO 80303
Tel: (303) 448 0727, Fax: (303) 448 7756
Email: messmer@txcorp.com

July, 2007

Distribution A: Public Release; Distribution Unlimited

Table of Contents

1 Introduction 1
2 The Plasma Simulation Framework VORPAL 1
2.1 Ionization Model 2
2.2 Fusion Reaction 3
2.3 Fusion of Shock-Accelerated Ions 4
2.4 Reverse Acceleration of Ions 8
2.5 Focusing of Reverse Accelerated Ions 9
2.6 D-T Acceleration in Shaped Targets 11
2.7 Neutron Generation in Shaped Target 14
3 Summary 16
4 Conclusions 17
5 References 18

List of Figures

Figure No. **Page**

1 Left panel: Example of a VORPAL Simulation, (Superconducting RF Cavity). Right Panel: Mono-Energetic Electron Beam Generated by Laser-Wakefield Acceleration 2

2 Left: Comparison of an Oxygen Spectrum Computed with the Kinetic Ionization Model in VORPAL [bars] with an Observed Spectrum [red stars]. 3

3 Energy Dependent Cross-Section for the D-T Fusion Reaction Based on the Model in [6] 4

4 Phase Space Projections of the D (blue) and T (red) Ions at Different Times 5

5 Spatial Energy Distribution of the D (blue) and T (red) Population after 0.48ps (left) and 0.96ps (right) for a Laser Intensity of $I=1.8 \cdot 10^{17}$ W/cm^2 6

6 Phase Space Projection (left) and Ion Energy (right) for the Interaction of a 60 fs, 2.6 10^{17} W/cm2 Laser Pulse with a D-T Plasma 6

7 Left: Temporal Evolution of the Nneutron Flux Generated in the Interaction of a 60 fs Laser Pulse with a D-T target. Right: Scaling of the Peak Neutron Flux with Increasing Laser Intensity 7

8 Reverse Acceleration of Ions in a Two Material Configuration 7

9 Ion Phase Space, x-y-v_x, Showing an Iso-Density Surface for He^{2+} ions (yellow) and Al^+ ions (green). 8

10 Flow Field of Reverse Accelerated Ions 9

11 Two Different Views of the Ion Density after 1.18 ps. 10

12 Evolution of the Ion Density over Time 11

13 Setup of Shaped Target Configuration: A High Density Shaped Tin Target (red) is Coated with an Under-Dense Deuterium Film (green) with a Tritium Ball (blue) Suspended in the Center of Spherical Mirror 12

14 Time Evolution of the D and T Density for a Laser Amplitude of E=3e12V/m (left) and 6e12 V/m (right) after 0.1ps (a), 0.3ps (b), 0.6ps (c) and 0.9ps (d). 13

15 Deuterium (left) and Tritium (right) Density Distribution after 1.33 ps for a Peak Electric Field of E= 3TV/m. 14

16 Time Evolution of the Neutron Generation for a Laser Amplitude of E=3e12V/m (left) and 6e12 V/m (right) after 0.3ps (a), 0.6ps (b) and 0.9ps (c) 15

17 Neutron Flux Evolution for Laser Amplitudes E=1.5 TV/m (dash-dotted), E=2 TV/m (dash-triple-dotted), E = 3 TV/m (solid) and E = 6 TV/m (dashed) 16

Glossary

1D	one-dimensional
2D	two-dimensional
CFL	Courant Friedrichs Lewy
D-D	Deuterium-Deuterium
D-T	Deuterium-Tritium
PIC	Particle-in-Cell
PML	perfectly matched layer
RF	radio frequency
TNSA	Target Normal Sheath Acceleration
VORPAL	Versatile Plasma simulation code

1 Introduction

Thermal neutrons with energies on the order of 0.025eV are of considerable interest to the Department of Defense and for commercial applications. Unlike high-energy photons, neutrons easily penetrate high density targets, but get effectively absorbed by low density materials like paraffin, nylon or explosives. This makes them attractive complements to X-rays for radiographic applications, e.g. for the detection or inspection of explosives inside steel casings. The key challenge is to develop a compact generator for thermal neutrons with a flux of at least 10^8 neutrons/cm^{2}s which is sufficient for radiographic applications.

The limited available amount of radio-isotopes like Californium 252, combined with the relatively short half-life, safety constraints and regulatory requirements make them unattractive for wide-spread use.

An alternative design exploits the Deuterium-Tritium (D-T) fusion, which generates Alpha particles and fast neutrons. In these sources, Deuterium ions are accelerated to about 130 keV and hit a Tritium target. In order to be attractive for radiographic applications, the 14.1 MeV neutrons have to be thermalized in an external moderator, for example a paraffin layer. This reduces the useful neutron flux by about two orders of magnitude. D-D reactions produce neutrons with lower energy (2.4 MeV), but one must also account for the branching ratio into charged products; i.e., d(d,p)t, and the reduced cross-section compared to d(d,n)α.

The acceleration of Deuterium ions is usually accomplished in a diode configuration. Recently, the interaction of high-power laser pulses with plasmas or solids has attracted considerable interest for the acceleration of electrons or ions [1, 2]. Especially the acceleration of ions to MeV energies opens entirely new possibilities for small scale ion accelerators and possibly for neutron sources.

In this project, we therefore investigated different target configurations for the potential use as neutron generators via numerical simulations.

2 The Plasma Simulation Framework VORPAL

The versatile plasma simulation code VORPAL [3] was originally designed for the investigation of laser wakefield acceleration of electrons. However, the code design is sufficiently general that it is capable to address entirely new application areas, like modeling of superconducting RF cavities, breakdown phenomena in microwaves guides or investigations of astrophysical plasmas. Figure 1 shows examples of such simulations. The code has recently been enhanced by a variety of models, including ionization processes.

The model for ionization processes is a hybrid between classical particle-in-cell [4] and the Direct-Simulation Monte-Carlo model [5]. Particles are pushed in their self-consistent

electromagnetic field. At every time-step, particles within a cell are considered for possible collision (and therefore reaction) by Monte-Carlo methods. The main parameters required in this model are energy dependent cross sections for ionization. While the model was mainly designed for ionization processes, it can relatively easily be adapted to other reaction types, including fusion.

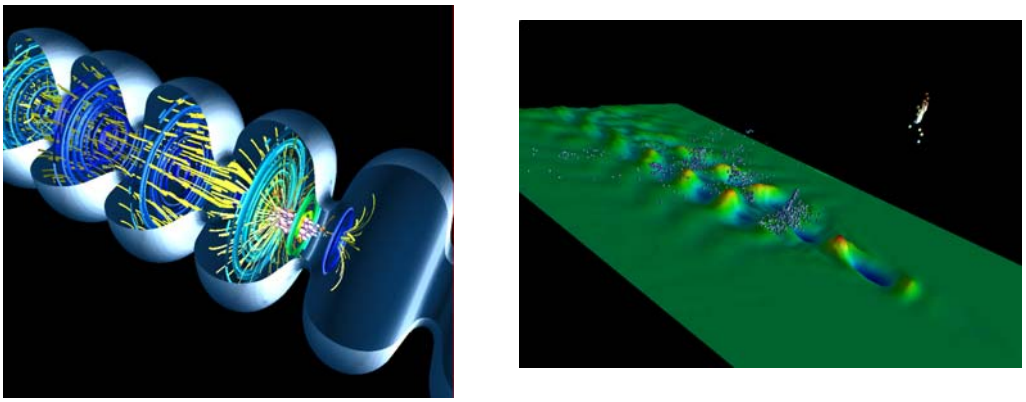

Figure 1: Left panel: Example of a VORPAL simulation, (superconducting RF cavity). Right Panel: Mono-energetic electron beam generated by laser-wakefield acceleration (Simulation by John R. Cary, Visualization: Peter Messmer).

2.1 Ionization Model

The ionization model in VORPAL was successfully used to reproduce ion spectra in Electron-Cyclotron Resonance Sources. Figure 2 shows a comparison of the kinetic impact ionization model in VORPAL with a spectrum for a hot population of oxygen measured at VENUS [7]. For experimental reasons, the spectrum was not measured for pure oxygen, but rather a mixture of Oxygen and Helium. The resulting spectrum at mass/charge ratios of 4 was therefore a blend between the oxygen and the helium contribution. The VORPAL simulation is a fully periodic box, containing atomic Oxygen, O^+ and e^-. The evolution of the different charge states is shown in Figure 2 (right). For the given electron energy, the first charge state not present in the initial distribution is going to be O^{2+}, but as soon as it is available in high enough concentration, the next ionization state is being produced and the ionization rate of O^{2+}drops. The overall spectrum obtained by integrating the ionization rates in time is shown in the left panel. For comparison, the measured current at VENUS [8] is shown. Good agreement is obtained for 5 charge states. As mentioned previously, the charge state M/Q=4 is mixed in the measured spectrum. We therefore plotted a token value of 0 at M/Q=4. The good agreement of the simulated with the measured spectrum indicates that the kinetic ionization model in VORPAL works as expected.

The energy dependent cross-sections for the ionization model in VORPAL are based on the semi-empirical model by Shull and Van Steenberg [9], which originates from the astrophysics community. This models predicts the energy dependent cross-sections of light elements, including, C, N, O, Ne, Mg, Si, S, Ar, Ca, Fe, and Ni.

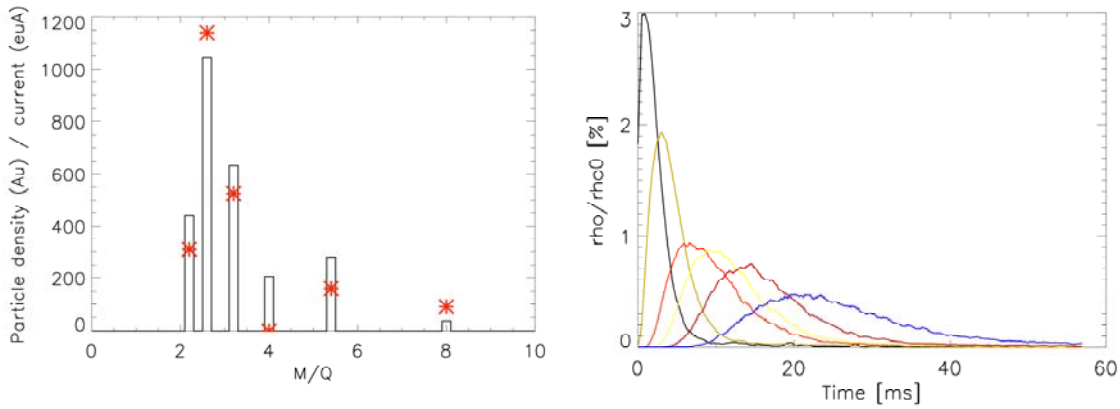

Figure 2: Left: Comparison of an oxygen spectrum computed with the kinetic ionization model in VORPAL [bars] with an observed spectrum [red stars]. The measurement at Oxygen 4+ was blended with Helium and therefore not shown in the picture. Right: Temporal evolution of the different charge states of Oxygen for a population starting with pure Oxygen. and O^{+}: O^{2+} (black), O^{3+} (brown), O^{4+} (organge), O^{5+} (yellow), O^{6+} (purple), O^{7+} (blue).

2.2 Fusion Reaction

The first part of this project was to implement a cross-section model for fusion reactions into VORPAL. Due to the relatively large cross-section at low energies, we chose the Deuterium-Tritium (D-T) reaction for all further studies. We chose a parameterized cross-section model [6] of the form

$$\sigma_T(E) = \frac{A_5 + \left[(A_4 - A_3 E)^2 + 1\right]^{-1} A_2}{E\left[\exp(A_1 E^{-1/2}) - 1\right]} \tag{1}$$

with A_1 = 45.95 barn keV, A_2 = 50200 barn keV, A_3 = 3.98e-3 keV^{-1}, A_4=1.297 and A_5=409 barn keV, and the total cross section σ_T measured in barn (10^{-24} cm^2) and the energy E in keV.

Figure 3 shows the cross-sections as a function of energy. The peak cross-section is on the order of 10^{-27} m^2, centered around an energy of 130 keV.

One of the main differences between the kinetic ionization model and the fusion model is the magnitude of the cross-section, which is about 7 orders of magnitude smaller for fusion than for ionization. We therefore did not track the generated ^{4}He (α particles) in the simulation, but rather estimated the number of neutrons generated in the interaction based on the particle statistics. This de-coupled approximation is valid because the α-particles are too few to have an impact on the plasma dynamics (i.e. energy deposition), despite the short mean free path at such high densities.

2.3 Fusion of Shock-Accelerated Ions

It has previously been reported that the interaction of a femto-second laser pulse with over-dense plasmas can lead to the formation of a shock wave in the target and to the acceleration of ions at this shock front [10]. In a target consisting of a D-T mix, this will therefore lead to a population of D-T ions streaming through a D-T background. If the energy of the shock- accelerated ions is large enough compared to the background ions, one expects that fusion reactions and therefore neutron generation will occur in the vicinity of the shock front

In order to test this hypothesis, we modeled the interaction of a femto-second laser pulse with a slightly over-dense D-T target. We assumed a plasma of density $2.8 \cdot 10^{27} m^{-3}$ being irradiated by a 60 fs, 0.8 μm laser pulse with an intensity of $I=1.8 \cdot 10^{17}$ W/cm^2 and a spot radius of 3 μm. The plasma was over-dense with a ratio of $n/n_{cr} = 1.6$. The plasma was modeled in a 2D configuration on a 3000 x 5 cell grid. The grid resolution in longitudinal direction is 1.6 nm and 10 nm in transverse direction. Perfectly matched layer (PML) boundary conditions were employed along both directions of propagation and periodicity was assumed in the transverse direction.

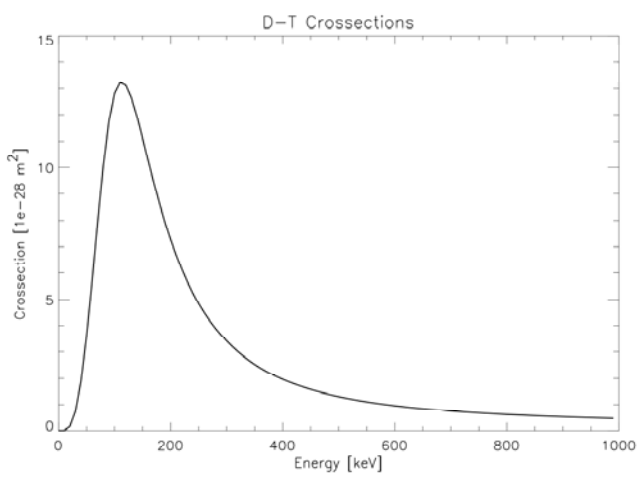

Figure 3: Energy dependent cross-section for the D-T fusion reaction based on the model in [6]. The peak cross-section is around 100 keV and reaches 10^{-27} m^2 (10 barn).

Figure 4 shows phase space projections of the interaction at different times. Due to the lighter mass, the Deuterium ions get accelerated to higher velocities than the Tritium ions. The Target Normal Sheath Acceleration (TNSA) mechanism accelerates both D and T ions at the backside of the plasma (at x=2.5 μm). However, in addition to the TNSA, particles are accelerated in the interior of the plasma at the shock front. This results in a fast population of D (and T) propagating forward through the background plasma.

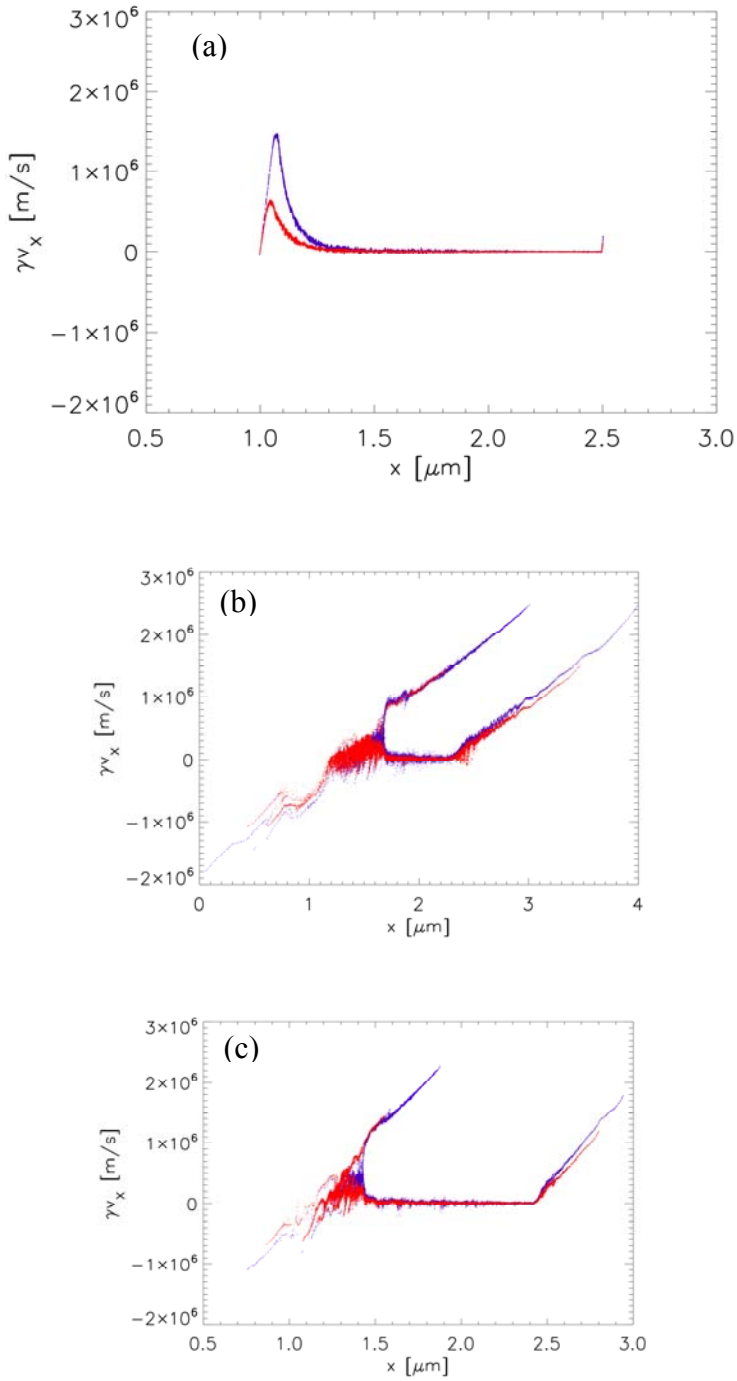

Figure 4: Phase space projections of the D (blue) and T (red) ions at different times: (a)- 96fs, (b)-0.48ps and (c)- 0.96ps.

Figure 5 shows the energy distribution of the ions for the above parameters. While these simulations demonstrate that a fast population of D can be generated by the laser-plasma interaction, the resulting ion energies are only on the order of 50 keV, for which the cross-section (see Figure 3) is too small to generate any significant number of fusion events.

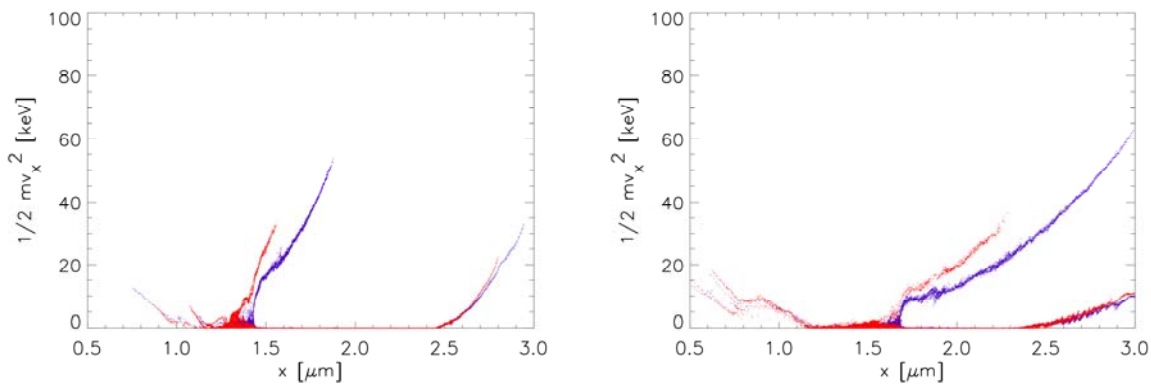

Figure 5: Spatial energy distribution of the D (blue) and T (red) population after 0.48ps (left) and 0.96ps (right) for a laser intensity of $I=1.8 \cdot 10^{17}$ W/cm^2.

Figure 6 shows the ion phase space and energy of an interaction with increased laser intensity of $I = 2.6 \cdot 10^{17}$ W/cm^2. All other parameters are identical to the previous simulations. The energies of the shock-accelerated ions are well above the 120 keV required for a significant number of fusion events to occur.

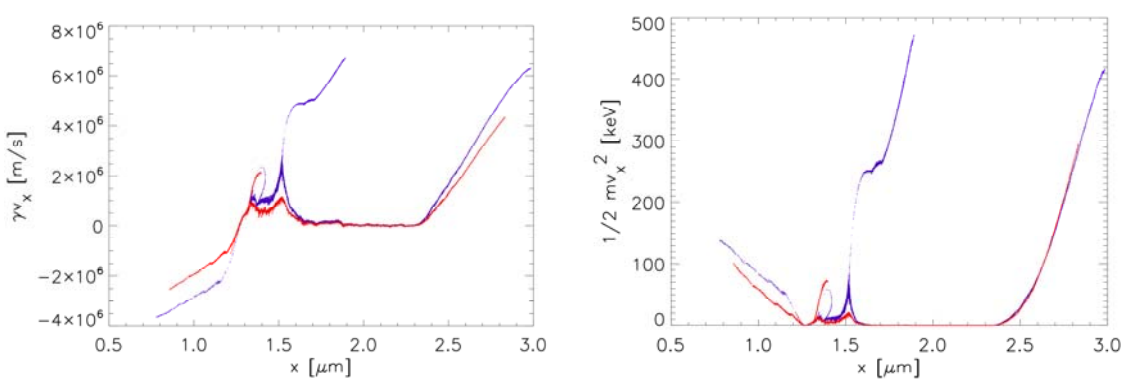

Figure 6: Phase space projection (left) and ion energy (right) for the interaction of a 60 fs, 2.6 10^{17} W/cm2 laser pulse with a D-T plasma.

Using the newly developed fusion model in VORPAL, we were able to investigate the neutrons generated in this interaction. Figure 7 shows the temporal evolution of these neutrons. The peak neutron flux occurs when the shock-accelerated ions propagate through the unperturbed plasma. Once they reach the former back side of the plasma, which is now accelerated via TNSA, the relative velocity is reduced and the number of fusion events is therefore reduced.

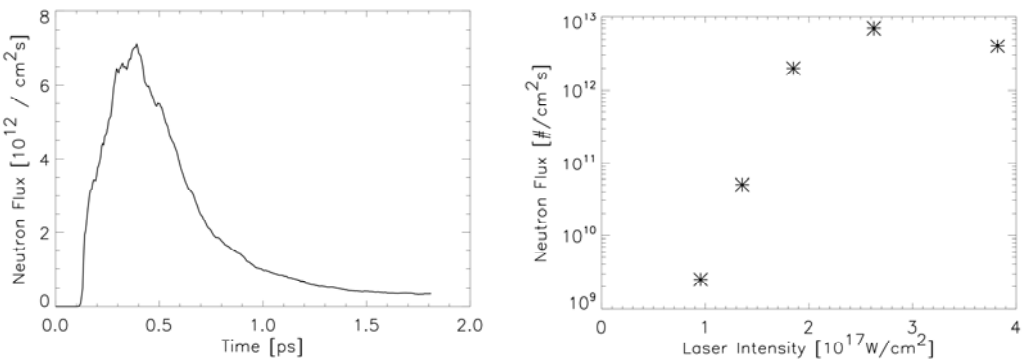

Figure 7: Left: Temporal evolution of the neutron flux generated in the interaction of a 60 fs laser pulse with a D-T target. Right: Scaling of the peak neutron flux with increasing laser intensity.

The energy of the shock-accelerated ions is highly dependent on the shock velocity, which is in turn dependent on the laser intensity. As these ions are responsible for the neutron generation, the laser intensity will control the neutron flux. Figure 7 shows the scaling of the peak neutron flux as a function of laser intensity. At intensities > $3 \cdot 10^{17}$ W/cm^2, the target was destroyed.

In summary, using the newly developed fusion model in VORPAL, we demonstrated that the interaction of high-intensity laser pulse with an over-dense D-T target can lead to the generation of neutrons.

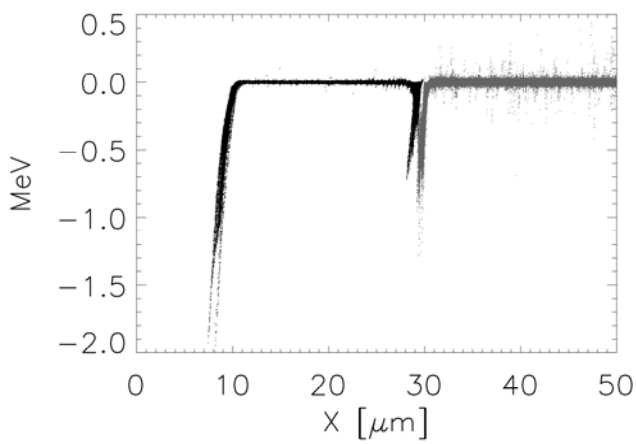

Figure 8: Reverse acceleration of ions in a two material configuration. Laser pulse entered from the left and accelerated the first population. At the interface of the two materials, plasma gets accelerated in backward direction.

2.4 Reverse Acceleration of Ions

While we demonstrated in the previous paragraph that the neutron flux generated by the interaction of a femto-second laser pulse with a D-T mix is sufficient for radiographic applications, one of the drawbacks of that configuration is the significant fraction of the D-T mix accelerated in the reverse direction (i.e. opposite to the initial laser propagation direction) which is lost to neutron generation. These back-propagating particles can be seen in the phase-space plots of Figure 4b-c, for $x < 1.5$ µm. A more efficient target design would take advantage of that ablated material as well.

One way of taking advantage of the ablated material is to optimize the target such that ions are only accelerated in the reverse direction. This can be accomplished by a target consisting of an under-dense coating applied to an over-dense material.

Figure 8 shows the ion phase space of such a two-component target, demonstrating the ion acceleration mainly in the reverse direction. This is an interesting and potentially important mechanism for this type of target, which was not previously investigated.

This mechanism is not limited to pseudo 1D simulations, but also works in 2D. Figure 9 shows the propagation of a 10^{21} W/m^2, 60 fs, 0.8 µm laser pulse in a Helium coated aluminum target. The simulation was run on a 640 x 320 cell grid, spanning a 64 x 32 µm domain. The neutral Helium is modeled as a gas at density of 10^{26} #/m^{-3}. The propagation of the laser pulse ionizes the coating and eventually accelerates the ions. This demonstrates that the reverse acceleration of ions also works in higher dimensions.

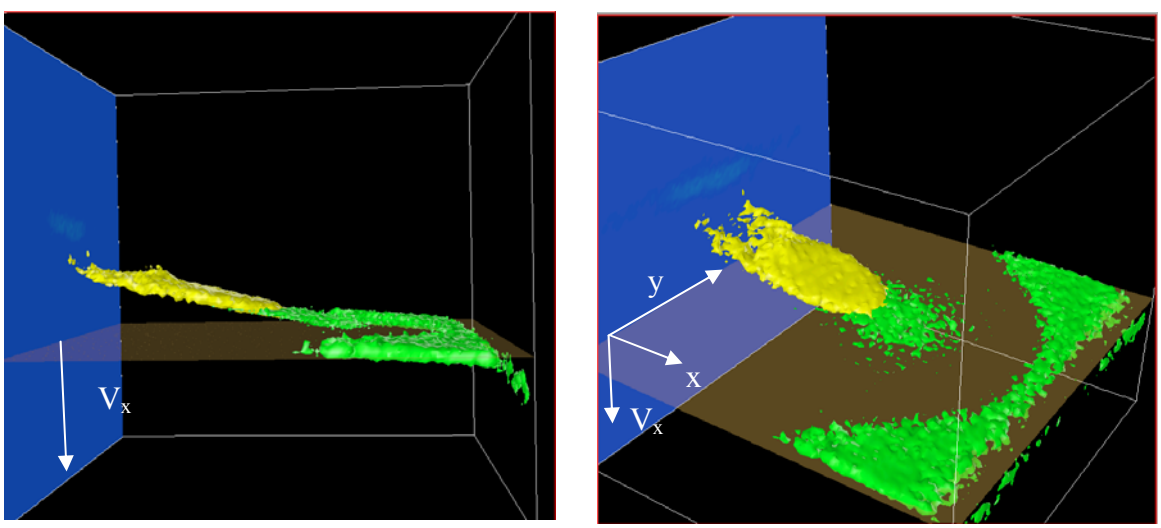

Figure 9: Ion phase space, x-y-v_x, showing an iso-density surface for He^{2+} ions (yellow) and Al^+ ions (green). Negative ion velocities are plotted upwards. The laser pulse initially propagates in positive x direction, gets reflected off the Al mirror and leaves the domain in negative x direction. The He^{2+} ions initially coat the inside of the spherical Al mirror and are accelerated in reverse direction by the laser pulse.

2.5 Focusing of Reverse Accelerated Ions

In this section we therefore investigate whether the material ablated in the interaction of a strong laser pulse with an over-dense target can lead to a neutron flux sufficiently large for radiographic applications. An alternative application for these reverse-accelerated ions would be to use them as a driver for e.g. Inertial Confinement Fusion. In particular, one may envision a combination of forward-accelerated (sheath mechanism) and reverse-accelerated ion beams created by the same laser pulse, operating on different sides of a target, to obtain synchronized beam-beam interactions. Additionally, one may also envision the target as spherically shaped, resulting in converging beams to increase density and temperature at the beam focal point; the target would then include holes through which the laser beam can pass, similar to Hohlraum targets.

We therefore start with investigating the possibility of converging ion beams from shaped targets. We ran simulations of a 10 μm thick foil, with a "dimple" on the near side having a radius of curvature of 5 μm. The plate is comprised of a neutral plasma with equal numbers of electrons and singly-ionized deuterium ions. Both plasmas have a density of $2.5 \cdot 10^{27}$ m^{-3}. The plasma frequency is $\omega_p = 2.825 \cdot 10^{15}$ rad/s and the initial temperature is 130'000 K, resulting in a Debye length of 0.866 nm. While this leads to numerical heating of the plasma, we anticipated that the violent laser-plasma interaction will dominate and provide at least some qualitative results. For more quantitative results, we then performed subsequent simulations at higher resolution.

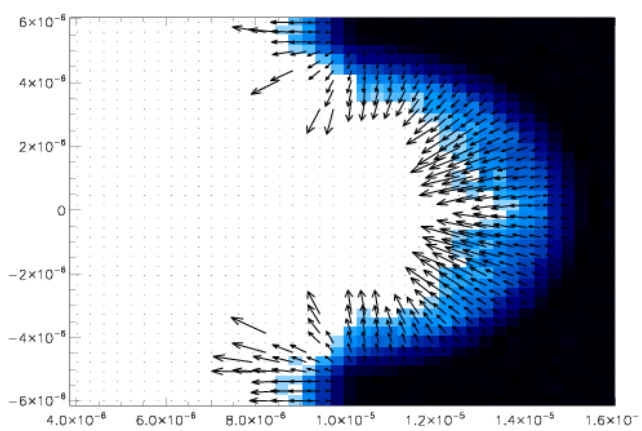

Figure 10: Flow field of reverse accelerated ions.

The laser has a wavelength of 0.8 μm, for which the plasma is slightly over-dense, $n/n_{crit}=1.44$. The laser field has a peak amplitude of $1.5 \cdot 10^{12}$ V/m (corresponding to an intensity of $3 \cdot 10^{17}$ W/cm^2) and a pulse duration of 20fs.

These initial simulations were run on a 3000x2000 cell grid spanning a physical domain of 30 μm x 20 μm (dx = dy = 10 nm), and a time-step of $1.73 \cdot 10^{-17}$s. Perfectly matched

layer boundary conditions were used along the laser propagation direction and periodic boundaries in transverse direction.

Figure 10 shows the Deuterium flow field after 1.73 ps (100'000 timesteps). The figure clearly shows the backward motion, as well as a focusing flow of the ablated material, which could eventually lead to a high density population in the center of the 'dimple'.

One of the key problems encountered in these simulations is the long timescale on which the interaction takes place. In addition, it would be highly useful to be able to fully resolve high density plasmas to avoid numerical heating, a common problem in Particle-In-Cell (PIC) simulations when the Debye length is not well resolved. In order to further investigate the focusing and to actually observe the formation of the focused ion population, we ran additional simulations, now with a finer grid resolution of 6000x4000 cells (dx =dy = 5nm) and a time-step of $1.17 \cdot 10^{-17}$s. In addition to the finer grid resolution, we also applied a [1 2 1] box-car filter to smooth each component of the current deposited by the charges at every time step. This resulted in a significant reduction of numerical heating and therefore enabled simulations on long timescales. Finally, we increased the laser pulse duration from 20 fs to 50 fs.

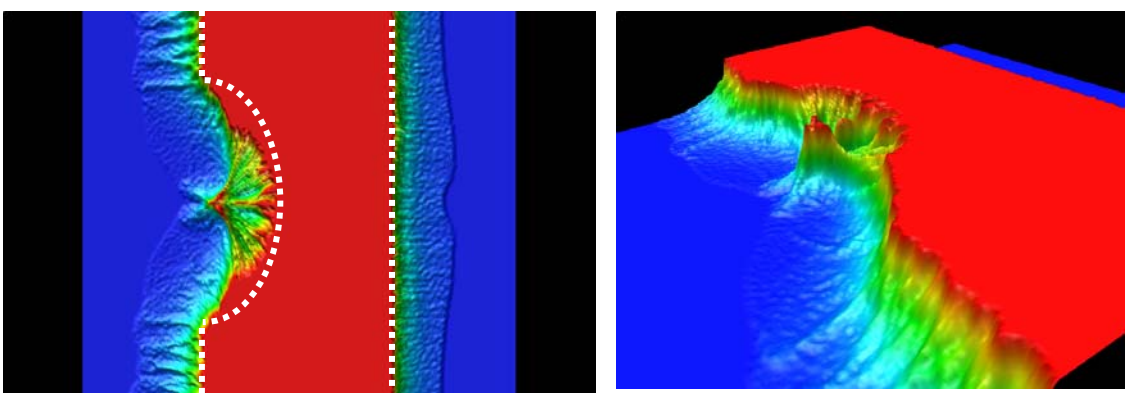

Figure 11: Two different views of the ion density after 1.18 ps. The laser pulse entered from the left, was reflected at the spherical mirror and left the domain to the left. The reversely accelerated ions form a high density population in the center of the mirror. The density of this population is significantly higher than the TNSA accelerated population on the right hand side of the foil. The boundaries of the initial distribution are shown as dotted lines.

The basic steps of the laser-matter interaction in these fully 2D simulations are essentially the same as in the pseudo 1D simulation in Section 2.3; i.e., TNSA. In this mechanism, the electric field of the laser pulse accelerates the electrons in the interaction region, which are rapidly accelerated into the target by the Lorentz force. The electrons stream through the foil and form a high-temperature, charged cloud out on the back side. The ambipolar field created by this cloud (sheath) accelerates the ions forward, while colder electrons are pulled back into the material (return current). If the laser pulse is long enough, the electrons return into the interaction region while the laser pulse is still on, being injected again into the foil (electron recirculation). At the same time, the ions in the interaction region start to move in reverse direction, due to the local positive charge left inside the target (reverse accelerated ions). See Figures 11 and 12.

While 1D simulations capture all these effects, they are unable to answer questions about the spatial distribution of the reversely accelerated ions, especially in a shaped target. They also do not properly capture effects from transverse gradients; for example, the return current at the periphery of the channel (outside the laser pulse envelope) can generate strong magnetic fields and affect the ion propagation.

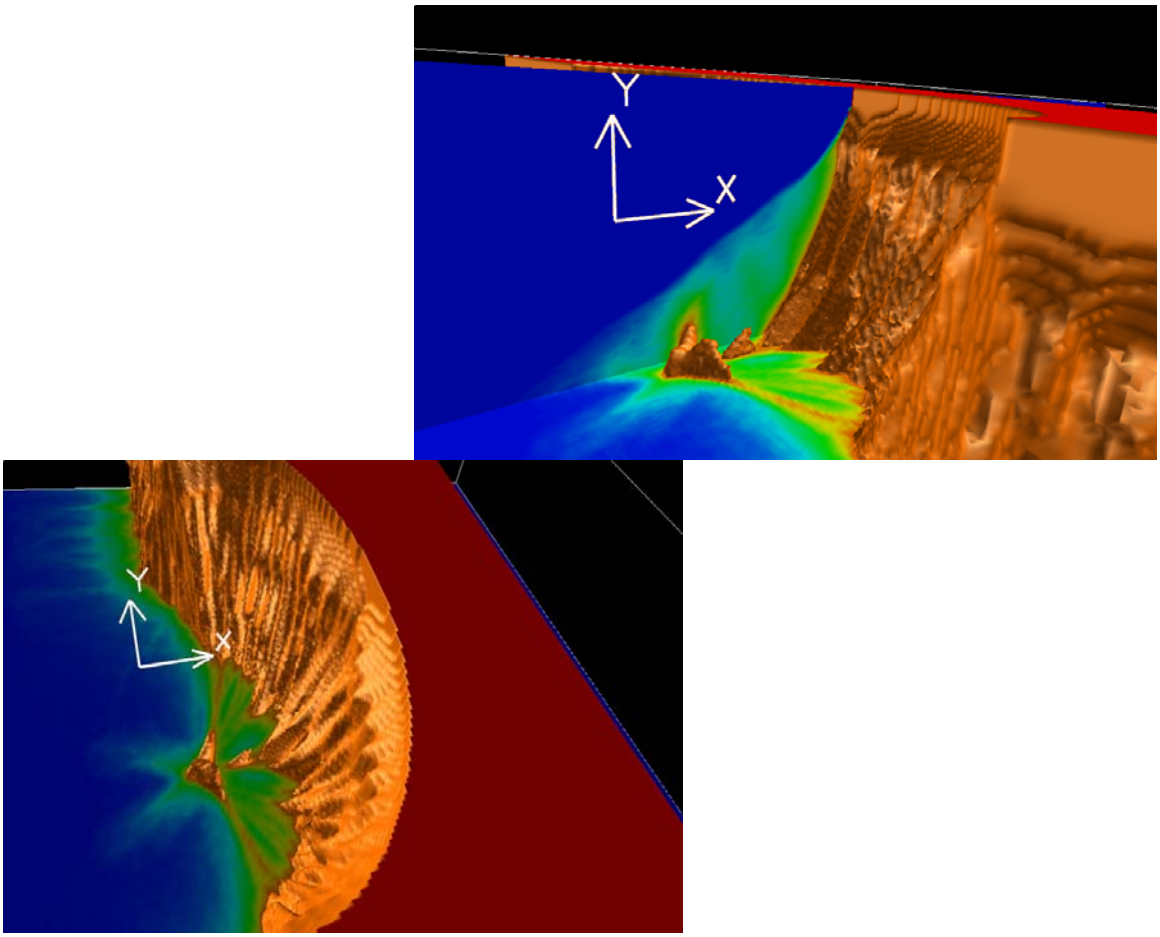

Figure 12: Evolution of the ion density over time. The laser pulse propagated along the x direction and got reflected at the spherical mirror. Time evolves in negative Y direction. The 'ripples' on the 'canyon-wall' show the strong filamentation of the ablated material. After about 1 ps, a high density population in the center of the mirror has formed, propagating in backward direction. This population shows strong divergence, most likely due to the high local space charge.

2.6 D-T Acceleration in Shaped Targets

While strong filamentation of the reverse-accelerated ion beam may prevent a good focusing for beam-beam interactions, we still need to examine the potential use of the reverse-accelerated material shown in the previous section as a driver for nuclear fusion. We tested a generic configuration where the reverse-accelerated ions can be focused onto a target. Figure 13 shows the overall setup: the main target consists of a 10 μm thick tin

foil at a density of $2.5 \cdot 10^{27}$ m^{-3} with a 5 μm hemi-spherical cavity in the center, which acts as a mirror. The cavity is coated with an under-dense, 2.5 μm thick Deuterium layer at a density of $4.4 \cdot 10^{26}$ m^{-3}. Suspended at the focus of the mirror is a Tritium ball with 2 μm diameter, also at a density of $4.4 \cdot 10^{26}$ m^{-3}.

The 0.8 μm laser has a spot radius of 2.5 μm and an intensity ranging between $1.5 \cdot 10^{21}$ Wm^{-2} and $2.4 \cdot 10^{22}$ Wm^{-2} corresponding to peak electric fields of 1.5 TV/m to 6 TV/m. The simulation domain is 30 x 20 μm covered by a computational grid of 6000 x 4000 cells and a simulation time-step of $1.06 \cdot 10^{-17}$s. Perfectly matched layer boundary conditions are applied in the laser propagation direction and periodic boundary conditions in the transverse direction. Similar to the simulations in the previous section, we chose an electron temperature which results in a Debye length resolved by the computational grid, as well as filtering of the currents in order to suppress numerical noise.

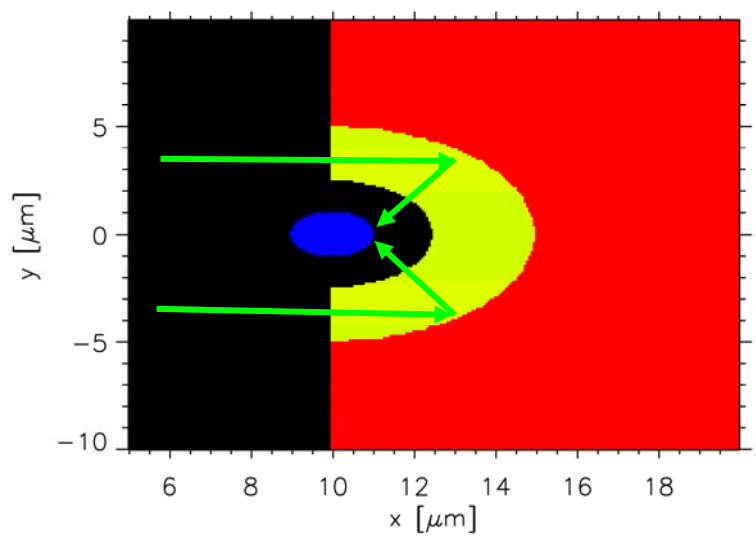

Figure 13: Setup of shaped target configuration: A high density shaped tin target (red) is coated with an under-dense deuterium film (green) with a Tritium ball (blue) suspended in the center of spherical mirror. The Tritium ball has a diameter of 2 μm, the Deuterium coating has a thickness of 2,5 μm. The cavity/mirror radius is 5 μm. The laser pulse enters from the left, is reflected off the spherical mirror and gets focused in the center of the mirror.

Figure 14 shows the development of the high density jet of ablated Deuterium. The over-dense lead foil, coated with the deuterium, is not shown. The peak density in the ejected Deuterium can reach up to 1.5 times the original Deuterium density. The Tritium ball explodes as a result of expulsion of electrons by the laser pulse (Coulomb explosion) and interacts with the counter-streaming Deuterium.

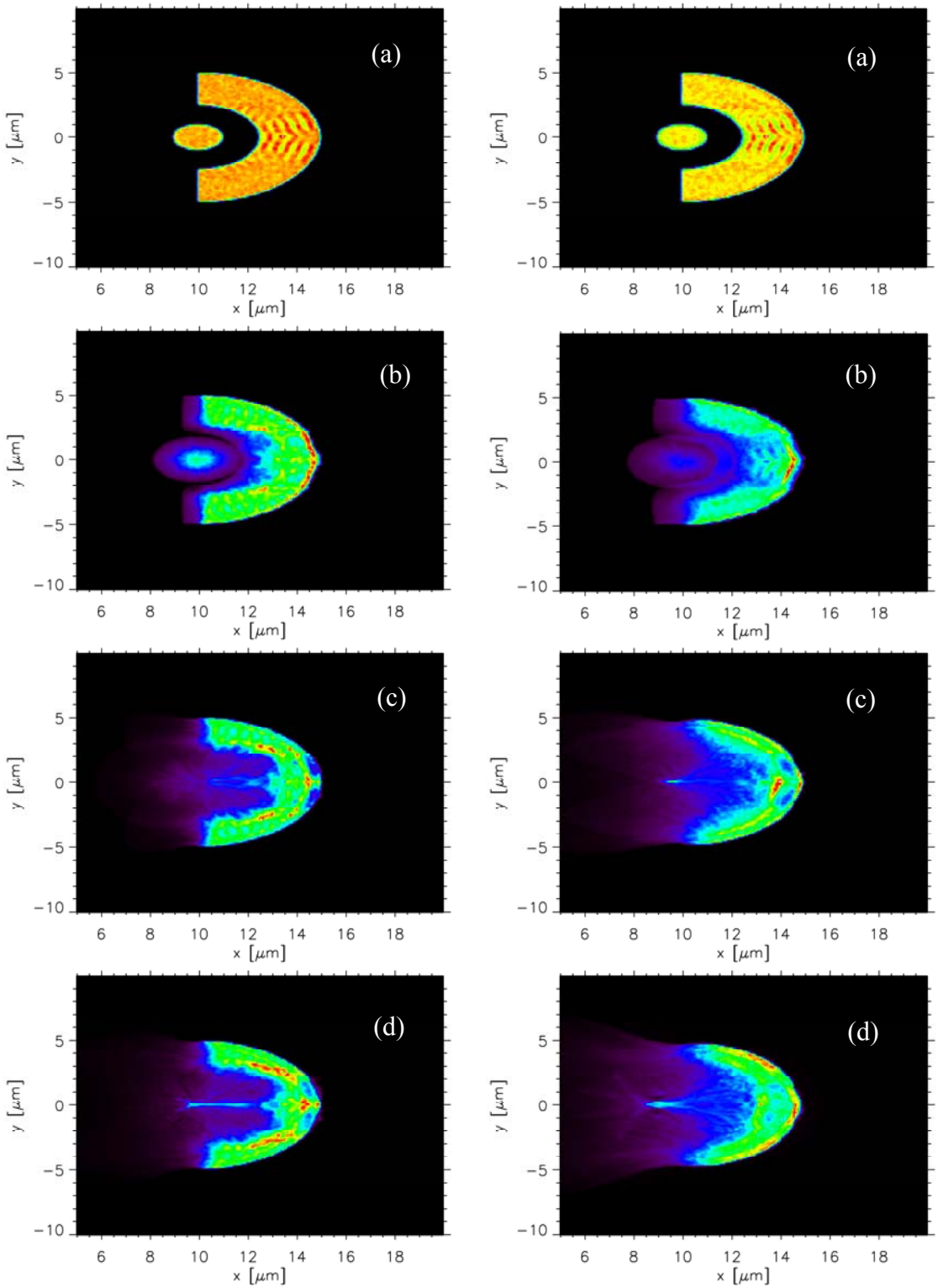

Figure 14: Time evolution of the D and T density for a laser amplitude of E=3e12V/m (left) and 6e12 V/m (right) after 0.1ps (a), 0.3ps (b), 0.6ps (c) and 0.9ps (d).

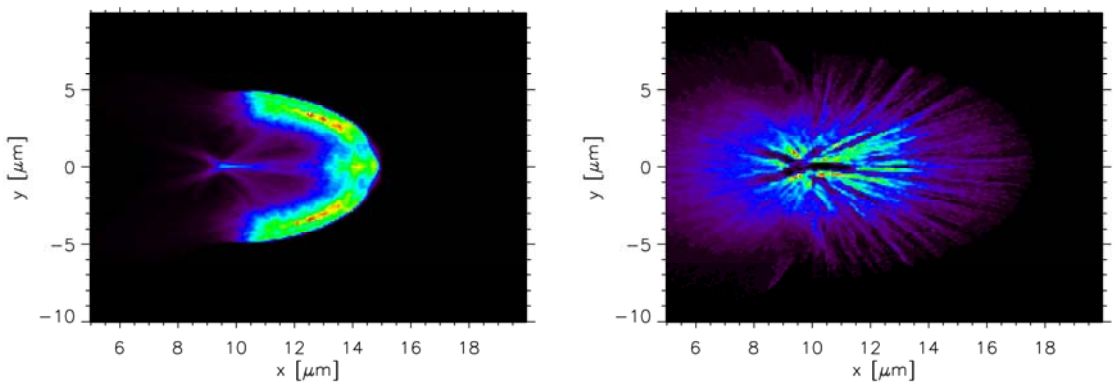

Figure 15: Deuterium (left) and Tritium (right) density distribution after 1.33 ps for a peak electric field of E= 3TV/m.

Figure 15 shows the Deuterium and Tritium density distribution after 1.33 ps. While at that time the reverse accelerated ions form a high density peak at the original location of the Tritium ball, the Tritium has been spread over a large volume due to Coulomb explosion.

2.7 Neutron Generation in Shaped Target

While the previous paragraph has shown that the ablated material in a shaped target can be focused and generate a high density peak, it remains to be seen whether the accelerated ions have the right energy to undergo fusion.

Figure 16 shows the temporal development of the neutron generation inferred from the Deuterium and Tritium densities and local mean velocities for two different laser amplitudes. For both amplitudes, neutron generation initially happens where the ions from the Coulomb explosion of the Tritium ball penetrate the Deuterium. Later, the interaction of the Deuterium jets creates another location of high neutron yield. Finally, the Tritium density at the original Tritium ball location becomes so low, that neutrons are no longer produced there.

Integrating the number of generated neutrons over the entire simulation domain allows estimating the total neutron flux as a function of time. Figure 17 shows the temporal evolution of the neutron flux for different laser peak electric fields. While increasing the laser peak field leads quicker to the generation of neutrons, the ions exceed the drift velocity of peak fusion cross-section. They therefore are lost to the generation of neutrons. On the other hand, for too weak a laser field, the accelerated ions are not fast enough and therefore do not lead to nuclear fusion. For the given configuration, a peak electric field of 3 TV/m maximizes the neutron flux.

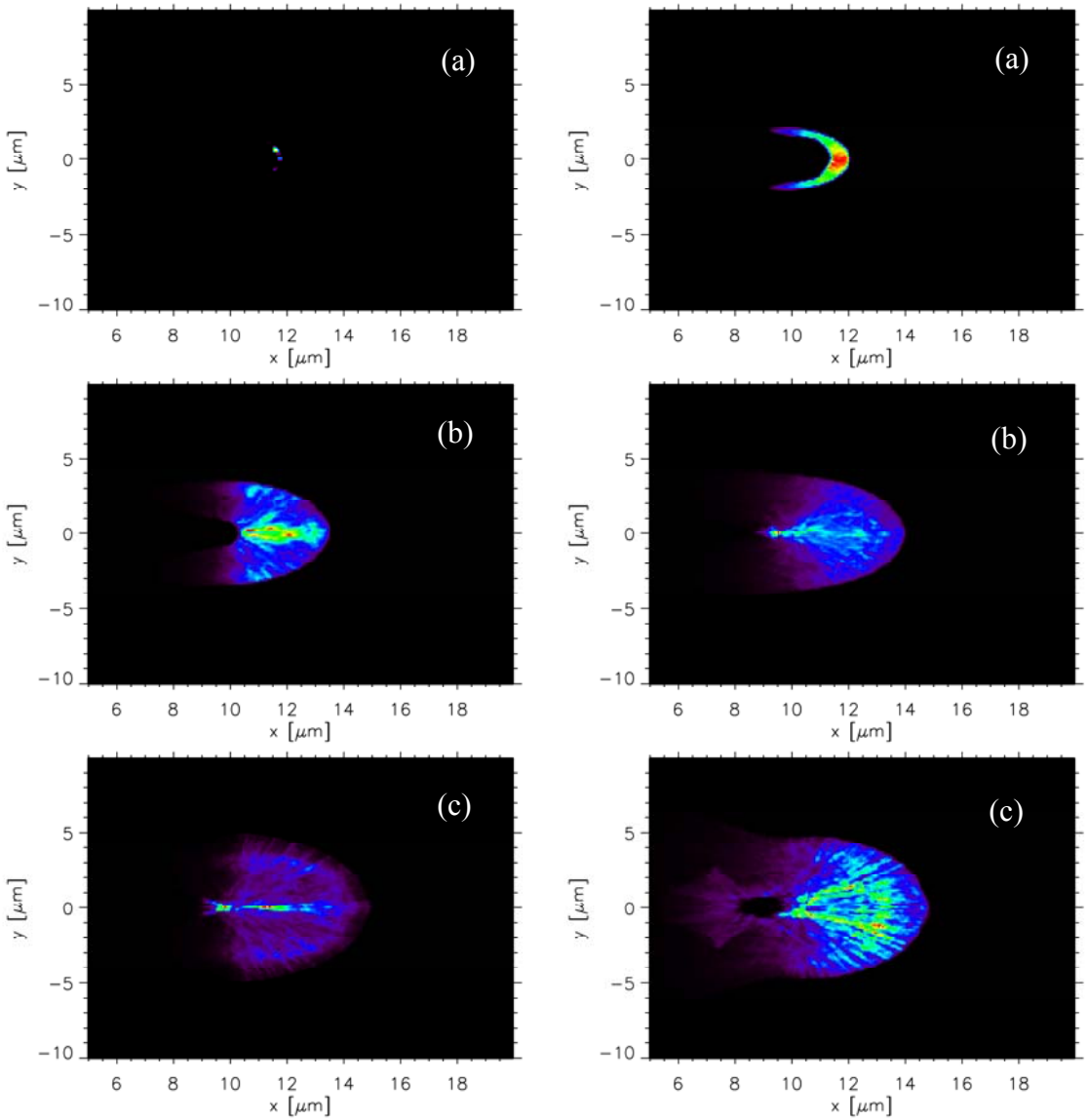

Figure 16: Time evolution of the neutron generation for a laser amplitude of E=3e12V/m (left) and 6e12 V/m (right) after 0.3ps (a), 0.6ps (b) and 0.9ps (c).

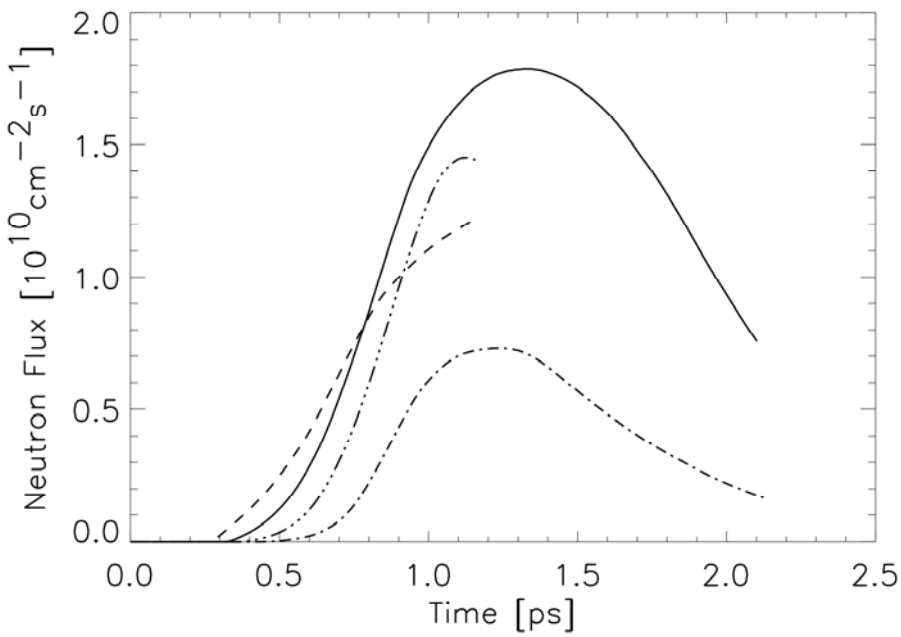

Figure 17: Neutron flux evolution for laser amplitudes E=1.5 TV/m (dash-dotted), E=2 TV/m (dash-triple-dotted), E = 3 TV/m (solid) and E = 6 TV/m (dashed). Increasing the amplitude leads to an increased momentum of the accelerated ions and therefore to a relative ion energy which is beyond the peak cross-section for the D-T fusion reaction.

The neutron flux in Figure 17 is computed at a distance of 1 m away from the target. Even assuming a reduction of the flux by about two orders of magnitude due to an external moderator should lead to a sufficient flux of neutrons for radiographic applications.

3 Summary

In summary, we found that ions ablated in the interaction of a strong laser pulse with an over-dense plasma can be focused by shaping the target. In case of a spherically shaped target, this leads to the formation of a high density ion population in the center of the spherical mirror. Target shaping has been successfully used to focus ions accelerated via TNSA on the backside of the target. These accelerated ions are then used as drivers for Inertial Confinement Fusion. Our simulations indicate that a similar population can be generated at the interaction site, leading to a drive beam traveling in the backward direction.

We have shown that the interaction of a femto-second laser pulse with a slightly over-dense target consisting of a D-T mix can be used to generate a neutron flux sufficiently large for radiographic applications. However, a large fraction of the D-T mix does not participate in the D-T fusion reaction and is therefore lost.

In a last configuration, the laser pulse was used to strip a Tritium ball from all its electrons. The resulting Coulomb explosion was used to accelerate the Tritium ions. The

reverse ion acceleration mechanism in a shaped target generates a counter-streaming population of Deuterium ions. Depending on the peak electric field of the laser pulse, a neutron flux large enough for radiographic applications can be generated.

The above simulations pushed 40 million particles on a 6000x4000 cell grid for about 110,000 time-steps and produced about 250 GB of data and took about 500 CPU days (12,000 CPU hours). Simulations of this size are too large for performing e.g. Parameter studies. One possibility to reduce the simulation time is to employ higher-order particle shapes, which interpolate the electromagnetic field not only from the surrounding cell, but from a more extended region in space. Using the field values from three neighboring cells, it is possible to relax the constraint to resolve the Debye length and only requires resolution of the electron inertial length. This results in a grid resolution which is lower by a factor $(c/v_{therm})^3$ which can easily exceed a factor of 1,000. In addition, this yields to an increased maximum possible time step due to its coupling via the CFL condition. Time savings of factors 10,000 and more can therefore be achieved.

4 Conclusions

In this project, we have implemented a kinetic model for nuclear fusion in the plasma simulation code VORPAL. We therefore extended a kinetic reaction model implemented in a different project by cross-sections for the Deuterium-Tritium nuclear reaction.

We investigated the interaction of a medium powered laser pulse with a slightly over-dense thin Deuterium/Tritium target. The interaction leads to the formation of a shock wave inside the plasma, which can accelerate particles at the shock front. This leads to the formation of a population of D (and T) streaming relative to a D/T background.

Using our newly developed fusion reaction model, we were able to compute the neutron flux generated in this interaction. The peak neutron flux was on the order of 10^{12} #/cm^{2}s, with a strong dependence on the incident laser pulse intensity.

While the overall number of particles per shot is relatively small due to the short interaction time, the high repetition rate of commercially available lasers with the required parameters can lead to high average neutron numbers.

Discussions with experimentalists have indicated that slightly over-dense thin targets can be realized using foams or gels or even using high-density gas jets. The simulation results therefore could be tested experimentally and possibly lead to the development of a compact neutron source.

We also performed simulations of reverse acceleration by laser-plasma interaction in shaped targets. We have demonstrated that a focusing of the ablated material occurs and leads to a high-density ion population propagating in reverse direction. This population could be used as a driver for Inertial Confinement Fusion.

Particle-in-Cell simulations of high-density plasmas are computationally highly demanding and algorithmic enhancements should be investigated. For example, higher order particle shapes have demonstrated that considerable time savings can be achieved compared to first order interpolation for particles.

5 References

[1] B.M Hegelich, B.J. Algright, J. Cobble, K. Killipo, S. Letzring, M.Paffett, H. Ruhl, J.Schreiber, R. K. Schultze, J.C. Frenandez, 'Laser acceleration of quasi-monoenergetic MeV ion beams', Nature, 439 (26), 441, 2006.

[2] C.G. Geddes C. Toth, J. Van Tilborg, E.Esarey, C.B. Schroeder, D. Bruhwiler, C. Nieter, J. Cary, and W.P. Leemans, Nature, 431, 538, 2004.

[3] C. Nieter, J.R. Cary, 'VORPAL: A versatile plasma simulation code', J. Comp. Phys, 196, 448, 2004.

[4] C.K. Birdsall and A.B.Langdon, 'Plasma Simulation Using Particles', New York, McGrawHill, 1985.

[5] G. A. Bird, 'Molecular Gas Dynamics and the Direct Simulation of Gas Flows', Oxford University Press, 1994.

[6] J.D. Huba, NRL Plasma Formulary, Washington DC, 2000.

[7] D. Leitner, C. M. Lyneis, T. Loew, O. Tarvainen, D. S. Todd, and S. Virostek, RSI **77**, 03A302 (2006).

[8] C. Lyneis, et al., First Results for the 28 GHz Operation o f the superconucting ECR Ion Source VENUS, Cyclotrons 04, 2004.

[9] M.J. Shull, M. Van Steenberg, Ap.J. Suppl., 48, 95, 1982.

[10] L. Silva et al., Proton Shock Acceleration in Laser-Plasma Interactions, PRL 92, 015002, 2004.

AFRL-RZ-ED-TR-2007-0065
Primary Distribution of this Report:

AFRL/RZSA (3 CD + 2 HC)
Jean-Luc Cambier
10 E. Saturn Blvd
Edwards AFB CA 93524

AFRL/RZSA (Original, with Signatures)
Record Custodian (Melinda Martindale)
10 E. Saturn Blvd.
Edwards AFB CA 93524

Peter Messmer (1 CD + 1 HC)
Tech-X Corporation
5621 Arapahoe Ave., Suite A
Boulder, CO 80303

Kevin Paul (1 CD + 1 HC)
Tech-X Corporation
5621 Arapahoe Ave., Suite A
Boulder, CO 80303

Peter Stoltz (1 CD + 1 HC)
Tech-X Corporation
5621 Arapahoe Ave., Suite A
Boulder, CO 80303

AFRL/RZ Technical Library (2 CD + 1 HC)
6 Draco Drive
Edwards AFB CA 93524-7130

Chemical Propulsion Info Analysis Ctr (1 CD)
Attn: Tech Lib (Mary Gannaway)
10630 Little Patuxent Parkway, Suite 202
Columbia MD 21044-3200

Defense Technical Information Center
(1 Electronic Submission via STINT)
Attn: DTIC-ACQS
8725 John J. Kingman Road, Suite 94
Ft. Belvoir VA 22060-6218